COMMUNICATION

Check for updates

Electrospun polymeric scaffolds enable 3D tissue-like functionality and efficient photoinduced contraction

Giulia Simoncini, [ID] [ab] Fabio Marangi,[b] Ilaria Venturino,[ab] Vito Vurro,[b] Andrea Bartolucci, [ID] [cd] Lorenzo Vannozzi, [ID] [cd] Ludovico Aloisio,[b] Martina Rossi,[e] Paola Moretti,[e] Chiara Bertarelli, [ID] [e] Giuseppe Maria Paternò [ID] *[ab] and Guglielmo Lanzani [ID] *[ab]

Muscle tissue engineering aims to develop functional muscle constructs with controllable contraction for applications in regenerative medicine and drug screening. In this study, we present the development of a biocompatible, light-responsive bio-hybrid construct, combining the electrospinning technique for scaffold fabrication with a phototransducer. The scaffold, composed of electrospun poly(vinyl alcohol) or poly(caprolactone) nanofibers, supports C2C12 myoblast adhesion and alignment, enabling the formation of organized cellular assemblies capable of generating measurable contractions. Light responsiveness is conferred by Ziapin2, a membrane-targeting azobenzene that enables non-genetic, optocapacitive stimulation under visible light exposure. We fabricated both 2D and self-standing quasi-3D scaffolds and systematically evaluated their mechanical properties and functional performance, observing that aligned fibers enhanced cellular organization and promoted macroscopic contractions in response to exogenous stimulation. After identifying PVA as the optimal material for quasi-3D scaffold fabrication, we evaluated the light-induced contractions, which generated strain and stresses of up to 4×10^{-4} and 3.3 kPa, respectively, leading to a contraction force of 460 μN. These results highlight the potential of aligned and photosensitized nanofiber scaffolds as biocompatible, optically controllable platforms for engineered muscle tissues, with applications in soft robotics, *in vitro* modeling, drug screening and regenerative medicine.

Introduction

Tissue engineering aims to develop functional tissues for applications in regenerative medicine, disease modelling, and drug testing. A central challenge in this field is the design of biomimetic scaffolds that provide appropriate structural guidance and mechanical support while enabling externally controlled actuation. In skeletal muscle systems, anisotropic organization and coordinated contraction are essential features that must be recapitulated to achieve tissue-like functionality.[1–3] Engineering muscle cells into functional tissues has recently gained significant attention, for healing injuries to the motor system and the neuromuscular apparatus, including cardiac muscle.[4–6] Muscle cells can be seeded onto various substrates or matrices, including hydrogels, elastomers and extracellular matrices, and their contractile motion can be harnessed for diverse functions, such as artificial muscles, pumping, sensing and locomotion.[6] Numerous studies have explored the cultivation of myoblasts in biocompatible matrices that replicate the stiffness, elasticity, and morphology of natural tissues. 3D-printed gels have been utilized as tridimensional scaffolds for the proliferation and stimulation of cardiomyocytes with external photovoltaic micro-devices.[7] However, the inherent localized stimulation represents a limitation in the effectiveness of this approach, while an extended stimulation can be provided by molecules dissolved in the cell culture medium. Moreover, despite mimicking mechanical properties of living tissue, such system does not provide a preferential alignment to the tissue, which has been demonstrated to be ideal for skeletal muscle cell differentiation and functionality.[8,9]

In particular, electrospun (ES) scaffolds are commonly utilized due to their structural resemblance to the native extracellular matrix (ECM).[10,11] The nanofibrous scaffolds obtained by electrospinning have morphological, mechanical and biochemical properties that promote cell adhesion and proliferation. These are essential for myoblast fusion and myotube formation.[12] Importantly, when the ES network is deposited along a preferential axis, it can promote cells' alignment. Furthermore, electrospinning enables the easy and versatile fabrication of nanofibrous sheets, which serve as biocompatible scaffolds that support and promote tissue-like cell organization.[13] All these factors are known

[a] *Dipartimento di Fisica, Politecnico di Milano, 20133, Milano, Italy*

[b] *Center for Nano Science and Technology, Istituto Italiano di Tecnologia, 20134, Milano, Italy. E-mail: giuseppemaria.paterno@polimi.it*

[c] *The BioRobotics Institute, Scuola Superiore Sant'Anna, 56025, Pisa, Italy*

[d] *Department of Excellence in Robotics and AI, Scuola Superiore Sant'Anna, 56127, Pisa, Italy*

[e] *Dipartimento di Chimica, Materiali e Ingegneria Chimica "Giulio Natta" Politecnico di Milano, 20133, Milano, Italy*

2832 | *J. Mater. Chem. B*, 2026, **14**, 2832–2842

This journal is © The Royal Society of Chemistry 2026

to contribute to the formation of aligned and functionally organized muscle tissues.

Once cells are grown and organized within the scaffold, their functionality depends on the availability of tools for exogenous contraction stimulation, with minimal side effects and invasiveness. To this end, photostimulation has recently gained attention as a method for regulating cellular activity with relatively high spatial and temporal resolution, selectivity, and less invasiveness compared to electrical stimulation, which remains however the most commonly used technique.[14] Several approaches have been developed to induce light sensitivity in cells,[15–17] including optogenetics,[18,19] as well as the use of organic[20–22] or inorganic semiconductor interfaces.[17] Optogenetics methods have demonstrated strong efficacy in initiating action potentials in activatable cells and have been successfully adapted for the light-controlled activation of cardiomyocytes and skeletal muscle.[18,23]

Instead, our approach relies on a materials-driven strategy: a membrane-targeting azobenzene molecule capable of triggering contraction in skeletal muscle cells upon light stimulation. Engineered muscle tissues with light-responsive properties could be utilized for regenerative therapies, particularly in cases of muscle degeneration or injury.[25] Additionally, these systems hold potential for high-throughput drug screening platforms, where controlled muscle contractions could serve as functional readouts.[26] Furthermore, in biohybrid robotics, engineered muscle actuators controlled by light could enable the development of soft, adaptive bio-machines.[27] Such an approach benefits from the fact that the mechanical properties of soft actuators more closely resemble those of biological tissues than those of rigid actuators, making them well suited for mimicking the functions of biological appendages, organs and tissues.[6]

Here we present biocompatible, ES scaffolds that support viability, alignment, and light-triggered contractions of organized C2C12 cellular assemblies. The scaffolds are fabricated by electrospinning poly(vinyl alcohol) (PVA) or poly(caprolactone) (PCL)[28,29] fibers and loaded with C2C12 cells. PCL and PVA were chosen as well-characterized, biocompatible, and biodegradable polymers, previously used for cell culture and in muscle cell studies.[30–32] After the formation of myotubes, light-sensitivity is conferred by adding a membrane-targeting molecular phototransducer, namely Ziapin2,[24,33] which induces cell excitation *via* an optocapacitive effect both *in vitro* and *in vivo*.[34–36] First, we assessed the functionality of 2D and quasi-3D networks with the final goal to create a tissue-like, free-standing muscle construct. PVA self-standing membranes were selected for optostimulation experiments in a quasi-3D configuration, as they combine a Young's modulus within the same order of magnitude as contracting skeletal muscle (~ 1 MPa)[37] with a high degree of alignment that supports robust myotube formation. Contractile responses of C2C12 under repeated visible-light stimulation were measured, revealing a stress of 3.3 kPa and a strain of 4×10^{-4}, accompanied by linear displacements of $\Delta L \approx 4$ μm and generated forces of approximately 460 μN. Such values highlight the importance of the need for three-dimensional

cellular organization to activate synergistic contractile behaviour. Additionally, by using electrospinning as a technique for developing contractile quasi-3D actuators, we achieve contractile stress values within the range reported for C2C12 3D constructs (1–50 kPa).[36,38] Intriguingly, photoinduced contractions are within the same order of magnitude of conventional electroinduced pacing, while offering the significant advantage of being far less invasive. By combining anisotropic scaffold architecture with photoresponsive membrane modulation, we establish a biohybrid platform capable of generating measurable contractile forces under optical stimulation. This approach links nanofabrication, soft-matter mechanics, and non-genetic photostimulation to create light-controlled, muscle-like constructs with potential relevance for soft bioactuation, *in vitro* modelling, drug screening, and regenerative medicine.

Experimental

Polycaprolactone solution preparation and electrospinning

The solution was prepared by dissolving PCL (Mw 80 000 Da) at a concentration of 12% w/v in a solvent mixture of chloroform and dimethylformamide (4 : 1 v/v) and stirred overnight at room temperature.

The solution was electrospun (ES) with an E-Fiber EF100 electrospinning system from Leonardino, through a 20 gauge (G) needle to produce randomly oriented and aligned nanofibers using different types of collectors. For both the 2D random and aligned configurations, to avoid fiber detachment from the substrate, the deposition was carried out on microscope glass slides (1 cm × 1 cm) with a spin-coated layer of PCL. The randomly aligned fibers were collected on a flat collector. The deposition process for 2D samples was carried out until a homogeneous layer of fibers formed on the substrate. The electrospinning parameters for random fibers were as follows: flow rate = 4 mL h^{-1}, distance from the collector = 15 cm, voltage = 20 kV, temperature = 21 °C, and humidity = 50%.

Aligned fibers were obtained using a rotating drum with the same solution concentration and the following parameters: flow rate = 1 mL h^{-1}, voltage = 30 kV, distance from the collector = 15 cm, rotation speed = 2000 rpm, temperature = 21 °C, and humidity = 50%.

For 3D self-standing ES membranes, we adopted longer deposition times, 15 minutes for random fibers and 1 hour for aligned fibers, while the other parameters were kept unchanged. However, fibers were collected on aluminium foil to allow their detachment. All samples were dried under a hood overnight and cut (1 cm × 1 cm) before use.

Spin coating of polycaprolactone films

The solution used for the fabrication of PCL (Mw 80 000 Da) films was prepared at a concentration of 5% w/v in chloroform. A small volume of the solution (125 μL) was spin-coated with an acceleration of 1500 rpm s^{-1} and a final speed of 3000 rpm for 50 seconds.

This journal is © The Royal Society of Chemistry 2026

J. Mater. Chem. B, 2026, **14**, 2832–2842 | **2833**

Polyvinyl alcohol solution preparation and electrospinning

Polyvinyl alcohol (PVA) electrospun fibers were prepared by dissolving Mowiol 18–88 (130 kDa) in deionized water at a concentration of 10% w/w. To ensure complete dissolution, the solution was maintained at 90 °C and stirred overnight.

Random fibers were obtained using a collector distance of 20 cm, voltage = 14 kV, and flow rate = 0.1 mL h^{-1}. For aligned fibers, the parameters were: rotation speed = 500 rpm, flow rate = 0.2 mL h^{-1}, collector distance = 20 cm, and voltage = 17 kV.

Fiber collection for 2D substrates followed the same method as for PCL. For self-standing membranes, the deposition time for both aligned and random samples was fixed at 1 hour and 45 minutes.

Polyvinyl alcohol fiber crosslinking

PVA samples require crosslinking to prevent fiber dissolution in water when used for cell culture. Crosslinking was performed by immersing the samples in a solution containing 0.2 M glutaraldehyde and 0.05 M hydrochloric acid in acetone for 1 hour and 30 minutes. The substrates were then washed three times with acetone, followed by deionized water, and left to dry overnight before use.

Scanning electron microscopy and alignment analysis

All scaffolds were deposited on silicon substrates and examined under a scanning electron microscope (SEM – Tescan Mira3) using secondary electrons and an accelerating voltage of 5 kV to evaluate fiber morphology and diameter. Fiber alignment was analysed using ImageJ software by measuring the angle formed between the fibers and the vertical axis of each image. The fiber angles were normalized from 0° to 90°.

C2C12 cell culture

C2C12 cells (ATCC) were cultured at 37 °C in a 5% CO$_2$ atmosphere, maintaining confluence below 70% to prevent damage. The cells were maintained through a maximum of 15 passages. The maintenance medium consisted of Dulbecco's modified Eagle's medium (DMEM) supplemented with 10% fetal bovine serum and 2% glutamine.

Cells were seeded at a density of 197 cells per mm^2 for the 2D samples configuration and 394 cells per mm^2 for the 3D self-standing membranes. Before cell seeding, the scaffolds were sterilized under UV light for 1 h and 30 minutes and the samples were coated with a fibronectin solution (1 : 200 in phosphate buffer without Ca^{2+} and Mg^{2+}) to improve cell attachment. Upon reaching confluence, the medium was replaced with a starvation medium composed of DMEM and 2% glutamine. After four days, differentiation was induced using a medium containing DMEM, 2% glutamine, and 2% Horse Serum for 2D samples, while 3D samples received 10% Horse serum[24] and insulin 1 : 1000 was added. Throughout the starvation and differentiation phases, the medium was refreshed every two days over a total duration of 12 days.

Confocal microscope images and fusion index analysis

Confocal microscope images have been taken by using an inverted laser microscope (Nikon Eclipse Ti2). Images were acquired using NIS-Elements (Nikon Imaging Software) with a 60× objective. Nuclei were stained with Hoechst (1 : 1000) and the cell membrane was stained with cell mask deep red (1 : 1000), which were incubated for 5 minutes in PBS and then washed off. To evaluate the fusion index, a 20× objective was used and image analysis was performed using ImageJ.

Optical stimulation

During the optical stimulation experiments, the cells were treated with Ziapin2 dissolved in dimetylsulfoxide (DMSO). Ziapin2 was directly added to the cell's media reaching a final concentration of 25 μM for 2D samples and 50 μM in quasi-3D self-standing membranes. The multi-well plate was incubated for 10 minutes to allow internalization of the photochromic molecules before transferring the cells into an extracellular solution. The incubation time for self-standing membranes was 30 minutes. The extracellular solution contained NaCl (0.14 M), KCl (0.0054 M), MgCl$_2$ (0.0018 M), CaCl$_2$ (0.0018 M), glucose (0.011 M), and HEPES (0.01 M).

Optical stimulation and visualization were performed using a Nikon Eclipse Ti inverted microscope equipped with a 470 nm cyan LED source. A 20×/0.50 objective (Nikon) was used to observe myotube contractions in the samples. Cells were stimulated by pulse trains at three different frequencies: 0.5, 1, and 2 Hz. Light pulses lasted 200 ms for 0.5 and 1 Hz stimulation, while for 2 Hz, the pulse duration was reduced to 100 ms. In self-standing membranes, only 1 Hz was used to photostimulate the myotubes.

Video recordings of the stimulation experiments were acquired using PVcam software. Stimulation began 20 seconds after video recording started and continued for several seconds beyond the end of the protocol to determine whether contractions were externally triggered or resulted from intrinsic biological activity. All experiments were conducted at 37 °C without CO$_2$ control.

Electrical stimulation of ES membranes

Electrical stimulation was performed by applying a 3 V voltage at a frequency of 1 Hz, with each pulse lasting 20 ms. The extracellular solution used during stimulation was the same as that previously reported for optical stimulation. All experiments were conducted at room temperature without CO$_2$ regulation.

Video analysis

Video analysis was performed using ImageJ and a MATLAB script. The script included a visual recognition algorithm based on the Kanade–Lucas–Tomasi (KLT) method, which tracks object movement across frames. The selected region of interest (ROI) was divided into subregions, and coordinates for each subregion were extracted.

To quantify myotube contractions, the initial resting position in each video was set as the zero point. The algorithm then

calculated the average displacement of each point relative to this reference. The analysis included measurements of the average displacement of the ROI, the contraction trajectory, and the average contraction duration and frequency, following the methodology described by Venturino *et al.*[14]

Mechanical characterization

The ES membranes were evaluated using stress–strain measurements to assess their mechanical properties. Before the measurement, the membrane thickness was measured using a Hirox digital optical microscope (HRX-01) using the Z-stack functionality. For the aligned substrates, the force was applied in the preferential direction of orientation of fibers through an Instron Mechanical Testing System (Instron, Norwood, MA, USA), equipped with a load cell of 10 N. The tensile tests were performed with a displacement rate of 1 mm min^{-1} until fracture. Young's modulus was calculated from the slope of the initial 5% of the stress–strain curve, considering the ratio of the applied load to the cross-sectional area.

Results and discussion

Electrospinning process and fiber characterization

Electrospinning was chosen because it provides straightforward control over fiber alignment, diameter, thickness and porosity, all properties known to influence myoblast alignment, fusion and contractile maturation. In our protocol, alignment was achieved using a high-speed rotating collector, whereas randomly oriented mats were collected on a static plate; increasing deposition time produced self-standing membranes with the thickness required for quasi-3D cell culture (see Methods for specific parameters). We selected PCL $(C_6H_{10}O_2)_n$ and PVA $(C_2H_4O)_n$ to sample complementary material chemistries: PVA for its higher wettability and cell-friendly surface properties, and PCL for its hydrophobicity and

slower degradation. These design choices were made *a priori* to produce bead-free, continuous fibers with micro-architectural features that promote contact guidance and volumetric infiltration.

The four SEM images in Fig. 1 are representative examples showing aligned *vs.* random fiber organization and the absence of beads. For the SEM analysis, a small number of fibers were collected on a silicon substrate to better evaluate their morphology, diameters, and fabrication quality. In the case of PCL fibers, to prevent fiber detachment and improve adhesion to the substrate, a PCL interlayer of 1057 ± 18 nm was spin-coated on glass. SEM analysis revealed smooth fibers, free of beads or defects, as shown in Fig. 1A and B. Slight differences in fiber diameter were observed between randomly oriented and aligned fibers of the same material. The measurement carried out on SEM micrographs showed in all cases a diameter of a few hundred nm, more specifically: 250 ± 16 nm for PVA-aligned, 225 ± 13 nm for PVA-random, 312 ± 64 nm for PCL-aligned, and 260 ± 38 nm in the case of PCL-random. (Fig. S1 and S2, SI) The angle distribution of the fibers was extracted and normalized from 0° to 90°, and represented in polar plots, where the radial axis indicates the percentage of fibers aligned in each direction. The results reported in Fig. 1 show, as expected, that electrospinning deposition on a fixed substrate leads to randomly oriented fibers (both PVA and PCL), as evidenced by the broad angle distribution and the standard deviation value: 28° ± 17° for PVA and 41° ± 21° for PCL samples. In contrast, the aligned samples show fibers oriented predominantly between 80° ± 4° and 88° ± 1° (for PVA and PCL, respectively).

C2C12 cells culture on 2D nanostructured substrates

Following morphological characterization, we evaluated 2D scaffolds made from both materials to identify the optimal substrate and fiber morphology for muscle-cell alignment and to determine which samples yielded the strongest myotube
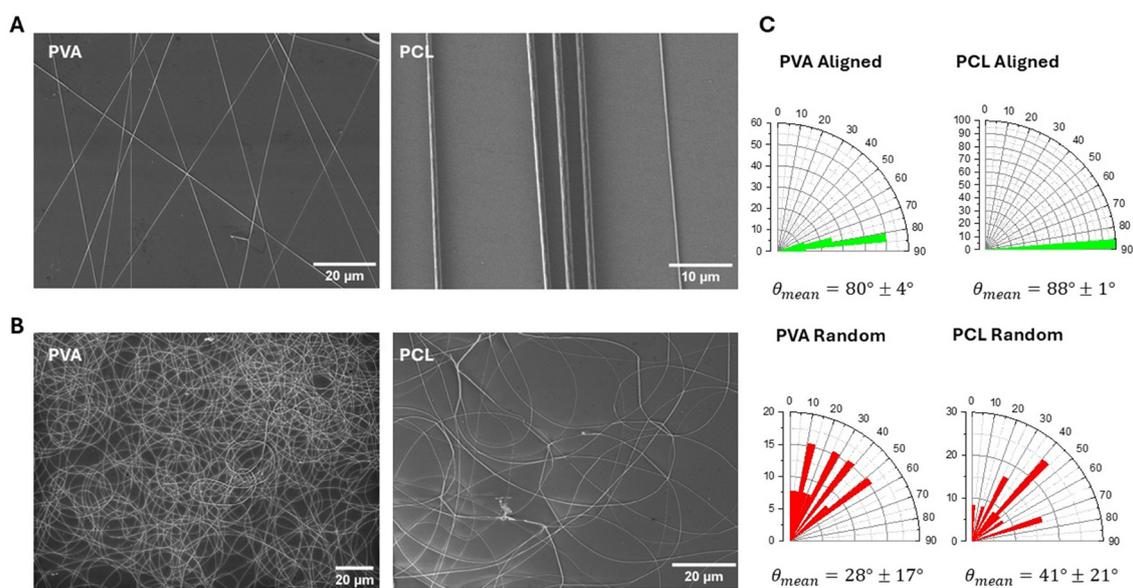

Fig. 1 SEM images of (A) aligned PVA and PCL fibers, (B) random PVA and PCL fibers, (C) alignment degree diagrams of each sample and mean angles.

contractions. Between 7 and 12 days after seeding C2C12 myoblasts, myotube formation was evident in all scaffold types (Fig. 2). Functional assays were then performed 12 days after the cells first reached confluence to ensure that the myotubes were sufficiently mature to contract.[39] Fig. 2 presents optical microscopy images of differentiated skeletal muscle cells cultured on aligned and randomly oriented ES PVA and PCL fibers. In the aligned scaffolds, myotubes clearly follow the orientation of the underlying substrate (Fig. 2A and B). Quantitative analysis, consistent with previous evaluations on neat ES networks, confirms the preferential alignment of myotubes in the oriented samples. Notably, myotubes exhibit an intrinsic tendency to align, as evidenced by a narrower angle distribution compared to that of the underlying fibers-even on randomly oriented scaffolds (Fig. 2E). However, the influence of fiber orientation extends beyond geometric guidance, affecting both cell proliferation and functional maturation. Samples with randomly oriented fibers exhibit a reduced number of myotubes compared to those with aligned fibers (Fig. 3E and F). Only in the presence of aligned ES scaffolds, we observe the formation of a homogeneous cellular layer containing myotubes that display spontaneous contractile activity. To assess the extent of cellular organization on the different substrates, we quantified the fusion index from confocal microscopy images, defined as the percentage of elongated, multinucleated cells containing more than two nuclei. Significant differences were observed among the substrates. The formation of elongated, multinucleated structures is commonly associated with myogenic progression in C2C12 cultures and is frequently used as a morphological indicator of myoblast fusion.[40] In addition, the observation of spontaneous contractions further supports the establishment of coordinated cellular assemblies. While fusion index and contractile activity are widely employed as functional and morphological readouts in engineered muscle systems, definitive confirmation of myogenic differentiation would require additional molecular analyses, such as immunostaining for lineage-specific markers (e.g., myosin heavy chain or actin)[41] and gene expression evaluation by PCR. However, comprehensive molecular characterization was beyond the scope of the present study, which is primarily focused on the design, fabrication, and functional evaluation of light-responsive nanofiber scaffolds as materials platforms for guided cellular organization. Notably, the fusion index analysis revealed substantial substrate dependent differences.[42] In the presence of aligned substrates, a higher fusion index was obtained compared to the random samples: aligned PVA showed the highest value of $62 \pm 8\%$, followed by aligned PCL with $48 \pm 12\%$. Randomly oriented PVA showed a fusion index of $30 \pm 3\%$, while randomly oriented PCL fusion index was $24 \pm 5\%$. All these values are represented in a box plot with the corresponding statistical analysis in Fig. S4 of the SI and some representative confocal images for each sample in Fig. S3. The pronounced increase in multinucleated cell formation observed on aligned substrates highlights the importance of nanostructured architectures that provide structural guidance through fiber anisotropy. Such alignment promotes parallel organization of myoblasts, facilitating end-to-end cellular arrangement and increasing the likelihood of membrane fusion events commonly associated with myotube development. The PVA promoted a higher fusion index compared to PCL. The superior performance of PVA may be attributed to its greater wettability and hydrophilicity compared to PCL.[43]
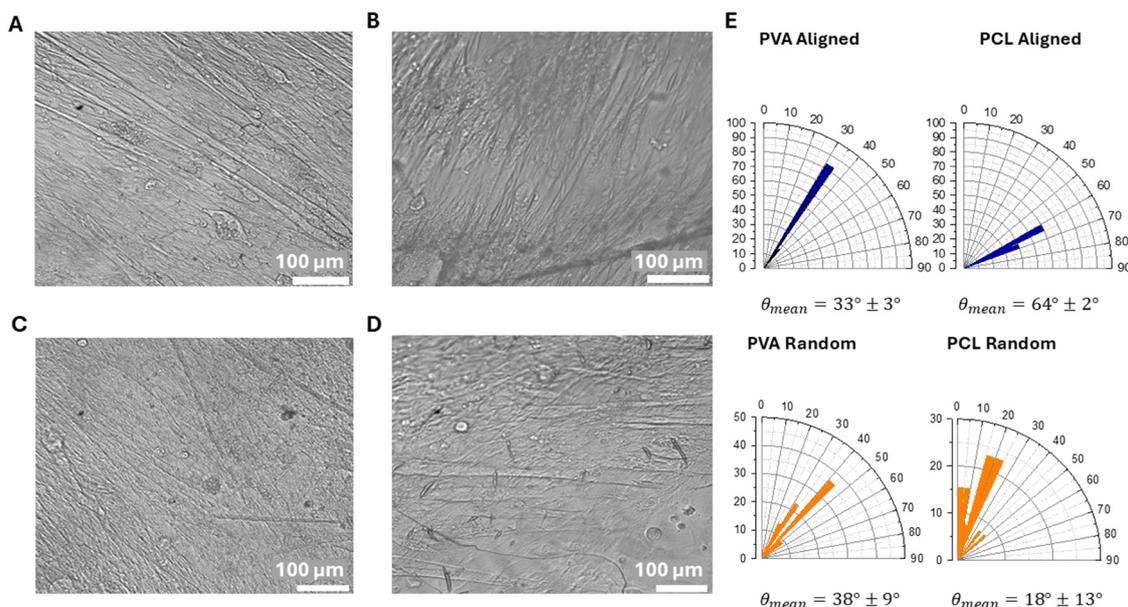

Fig. 2 Optical microscope images of myotubes on (A) PVA aligned substrates, (B) PCL aligned substrates, (C) PVA random substrates, (D) PCL random fibers. (E) Alignment degrees diagrams of myotubes differentiated on each sample and mean angles. The dimensions of all the 2D substrates were 1 cm × 1 cm.

2836 | J. Mater. Chem. B, 2026, 14, 2832–2842

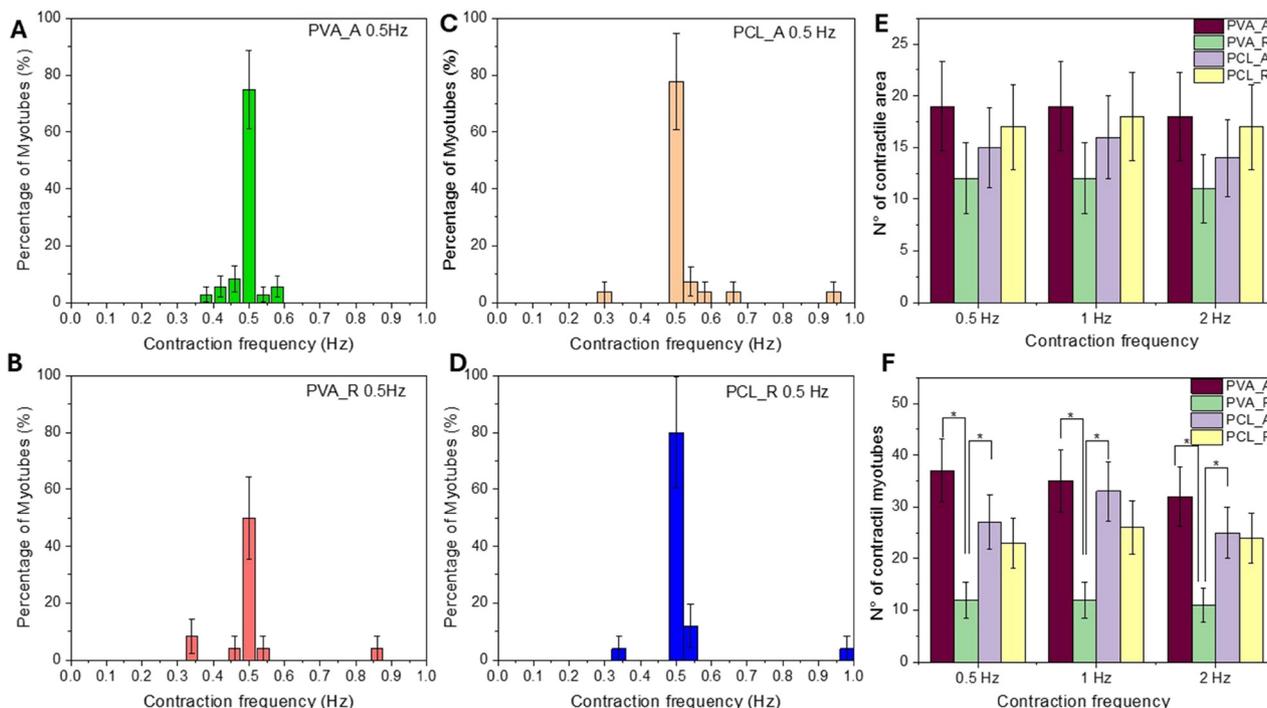This journal is © The Royal Society of Chemistry 2026

Fig. 3 Histogram represents the mean contraction frequency of myotubes photostimulated at 0.5 Hz in (A) aligned PVA 2D sample, (B) random PVA 2D sample, (C) aligned PCL 2D sample, (D) random PCL 2D sample. Bin sizes are based on the standard error of the frequency, whereas the error on the bar is $\sqrt{N}$%. (E) Histograms of the number of contractile areas in each type of sample at different light frequency stimulations. (F) Number of contractile myotubes in different types of fiber orientations at different light frequency stimulations. Six samples were analyzed for each scaffold in the analysis reported in E and F (the error bar is calculated as $\sqrt{N}$). All the samples were illuminated with a blue LED (470 nm) at a power density of 42 mW mm^{-2}. Student's t-test was performed as statistical analysis (*$p < 0.05$).

Muscle cell opto-stimulation

Opto-stimulation and contraction analysis

Differentiated C2C12 cells on 2D substrates were incubated with the amphiphilic azobenzene Ziapin2 to enable light-induced contractions. This molecule is designed to spontaneously partition into the lipid membrane through non-covalent interactions and modulate membrane potential *via* its *trans* → *cis* photoisomerization reaction. Briefly, upon partitioning, Ziapin2 tends to aggregate, leading to membrane thinning, hence an associated increase in capacitance. Photoisomerization disrupts these aggregates, restoring membrane thickness and producing a transient, reversible decrease in membrane capacitance. As demonstrated by Moschetta *et al.*,[44] Ziapin2 modulates strain-sensitive ion channels, which play a key role in excitation-contraction coupling.[45] The strain-induced opening of these channels causes transient potential hyperpolarization, followed by a rebound depolarization, sufficient to trigger an action potential. Although such a behaviour has proven to be general, as it has been observed in neurons, cardiomyocytes, skeletal muscle cells and bacteria,[46–49] the key novelty of this work is to provide a demonstration of Ziapin2-mediated optostimulation in 3D, tissue-like, muscle constructs supported by nanostructured, stretchable scaffolds. This advance is not a trivial extension of prior work: in moving to 3D, geometrically complex, nanostructured systems, the effectiveness of Ziapin2 could not be taken for granted. Being

a materials-driven paradigm, factors such as molecular aggregation, and light scattering can hinder isomerization and critically affect the optostimulation performances.

The cells were stimulated at 0.5, 1, and 2 Hz with 30-second light pulses trains with 200 ms pulse duration. The pacing efficiency was evaluated by working out contraction frequency distributions. These were extracted from videos recorded during photostimulation experiments using a 20× objective, and frequency analysis was conducted by a MATLAB algorithm employing visual recognition. The algorithm identifies and tracks myotube movement by selecting a region of interest (ROI) and following its displacement across each video frame. This approach enables extraction of the ROI position throughout the recording, allowing reconstruction of the myotube contraction profile.[24] In PVA-aligned samples, under 0.5 Hz stimulation (Fig. 3A) approximately 80% of the myotubes precisely followed the light stimulus. However, in randomly oriented PVA fibers (Fig. 3B), the percentage of myotubes contracting at 0.5 Hz dropped to 50%. In contrast, PCL samples maintained a similar percentage of myotubes (~80%) able to perfectly follow the pacing in both aligned and random fiber arrangements (Fig. 3C and D). It is worth mentioning that the increases in the stimulation frequency generally led to decreased myotube performance in both aligned and random substrates for PVA (Fig. S5 and S6 for PCL, SI). The number of contractile areas (regions containing actively contracting

This journal is © The Royal Society of Chemistry 2026

J. Mater. Chem. B, 2026, **14**, 2832–2842 | **2837**

myotubes) and the total number of contractile myotubes can be extracted from the videos and correspond to the number of ROIs where such activity is observed for each sample type. PVA-aligned scaffolds show the best performance, both in terms of contractile area count and myotube number (Fig. 3E and F). In contrast, PVA-random scaffolds exhibit nearly half of these values. A similar, though less pronounced, trend is observed in PCL scaffolds. The most pronounced differences were observed between PVA aligned and random substrates, whereas the differences between PCL and PVA did not reach statistical significance. These results may support the hypothesis that pre-aligning cells prior to differentiation enhances myotube maturation, as further evidenced by the fusion index analysis. In Fig. S7 of the SI, the mean contraction frequency analysis is also reported for the control samples, in which myoblasts were differentiated on a planar 2D surface without any nanostructure. These controls show a lower percentage of myotubes able to precisely follow the light stimulation frequency at each applied stimulation frequency.

Mechanical characterization of self-standing membrane in air

Aiming at increasing the volume of contractile tissue, as it happens in real muscular constructs, we then realized self-standing membranes by increasing the deposition time and keeping parameters and materials unchanged with respect to the 2D substrates deposition. The electrospun (ES) membranes were characterized by SEM to evaluate the presence of defects and the organization of the fibers (Fig. S9, SI). To evaluate the suitability of the ES membranes for C2C12 differentiation and their compatibility with cell contraction, the mechanical properties of the self-standing membranes in air were assessed by determining their Young's moduli. The thickness of the ES membranes used in the tensile test experiments was measured with a profilometer on three samples and found to be approximately 43 ± 15 μm for PCL aligned, 56 ± 8 μm for PCL random, 35 ± 3 μm for PVA aligned, and 53 ± 8 μm for PVA random (Fig. S10, SI). Fig. 4A compares Young's modulus (E) for both materials in aligned and random configurations obtained by

fitting the elastic region of the stress–strain curves shown in Fig. S11 (SI). The PVA random sample exhibits a Young's modulus that is almost one order of magnitude higher than the others, probably because the highly interconnected and entangled fiber network offers greater resistance to the applied force. All nanofibers' membranes are well suited for tissue engineering applications because their E values are in the 10–90 MPa range.[50] This turns out to be a distinct advantage of ES fibers, as in thin films, of both PVA and PCL, Young's modulus is in the GPa range.[51,52] Electrospinning also confers inherent porosity to the membrane, reducing material density for a given volume, thus increasing flexibility, and introducing defined surface topography.[53,54] Based on our comparative analysis, we therefore conclude that a combination of inter-related material properties, such as surface wettability, micro-structure/topography, and the local mechanical environment, mechanical properties and myotube density, fusion index, and light-responsive contractile performance, aligned PVA was the optimal material for fabricating tissue-like quasi-3D scaffolds. This choice was further supported by the absence of organic solvents during the fabrication process and the potential for future scaffold functionalization due to the presence of hydroxyl groups.

C2C12 proliferation and photoinduced contractile biomechanics of quasi-3D PVA scaffolds

Twelve days after seeding, we acquired confocal images to assess tissue-like cell distribution and proliferation. C2C12 nuclei were stained with Hoechst and cell membranes with CellMask Deep Red. In Fig. 4B and C, two representative cross-sections of the self-standing PVA membrane reveal the presence of cell nuclei distributed throughout the thickness of the material. This distribution demonstrates that cells did not remain confined to the surface but were able to migrate and populate deeper layers of the scaffold. Such infiltration indicates that the membrane architecture and porosity allow cell stacking and a quasi-3D tissue-like organization. In the SI (Fig. S8), we reported also the maximum and the minimum
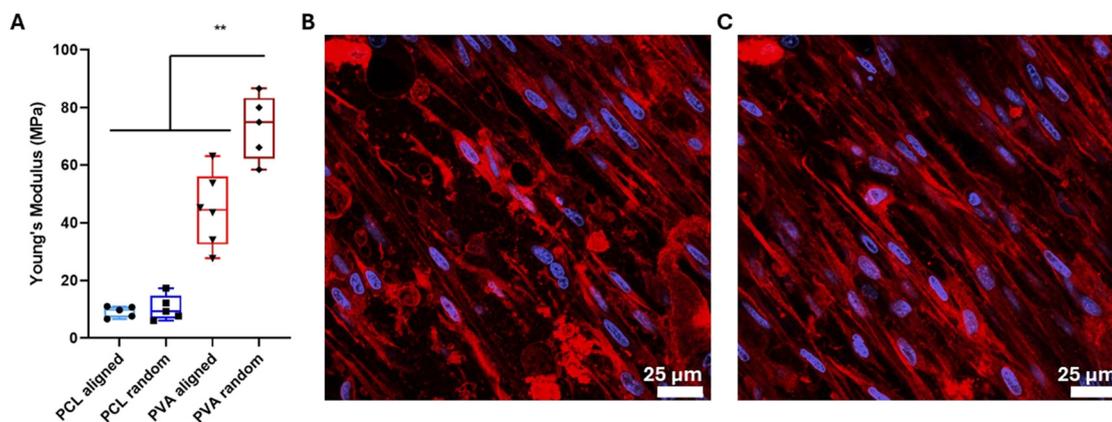

Fig. 4 (A) Comparison between Young's modulus of wet aligned and random fibers. (B) Image of the bottom focal plane from confocal z-stack, in blue myotubes nuclei, in red cells membrane. (C) Upper focal plane. In aligned samples the tensile strength was applied in the preferential fiber direction (anisotropic axis) and the random were treated as isotropic under the same test configuration.

2838 | *J. Mater. Chem. B*, 2026, **14**, 2832–2842

This journal is © The Royal Society of Chemistry 2026

intensity projection of the construct and a 3D image of the Z-stacked slices (Video S1).

To evaluate the contractile capabilities of this construct, we first applied conventional electrical stimulation before proceeding to the new photostimulation paradigm using Ziapin2. To observe the contraction, we employed a 20× objective, and the cell-seeded scaffolds were stimulated at 1 Hz (20 ms pulses, 3 V). Our PVA-based quasi-3D cell-seeded scaffold exhibited clear macroscopic contractions induced by a train of electrical stimuli at 1 Hz (SI Video S2). Having observed that standard electrostimulation drives a clear contractile behaviour, we then proceed to optical stimulation on samples sensitized with Ziapin2, noting well-defined and precise photoinduced contractions (SI Video S3).

Once the ability to contract under exogenous stimuli was demonstrated qualitatively, we performed a quantitative analysis of the contraction dynamics and mechanical actuation. Specifically, we calculated a photoinduced ES membrane displacement (ΔL_0) of 4 µm and, knowing the elastic modulus (E) of the membrane and its initial length (L_0) we could estimate the contraction-induced stress using the formula $\sigma = E\Delta L/L_0$ (with $\Delta L/L_0$ representing the deformation ε) and then obtained the force generated by the muscle tissue using the equation $F = \sigma A_{ef}$, where A_{ef} is the effective area. In the area evaluation, we considered the porosity of the ES membranes starting from value reported in literature of $\varphi = 0.6$[55] and the area was calculated as $A_{ef} = A_0(1 - \varphi)$ where A_0 is the area without voids. We used the effective Young's modulus of the sample measured after 12 days of incubation in the cell medium (DMEM), which turns out to be 8.26 MPa, a value that is sensibly lower than the 42 MPa measured under dry conditions (Fig. S12, SI). In terms of generated force, optical stimulation permits to reach a value of 460 µN and a stress of 3.3 kPa. All values used for calculation are summarized in Table 1.

These values significantly outperform typical stress values for 2D films, in the order of 0.5 kPa.[56] We attribute the effectiveness of our approach to the presence of a quasi-3D cellular organization and relatively high degree of alignment. In particular, literature reports that 3D constructs of C2C12 cells generate specific contractile stresses ranging from approximately 1 to 50 kPa, depending on the construct organization, substrate materials, degree of differentiation, and stimulation protocol.[36,38] It is also interesting to note that photoinduced contractions fall within the same order of magnitude as those produced by conventional electrical pacing ($\Delta L \approx 7.7$ µm; force ≈ 890 µN; stress ≈ 6 kPa see SI). Although direct comparison is challenging, given the different modes of stimulation and energy inputs, we evaluated the photo- and electrical-induced biomechanics both at maximum light intensity and the strongest electrical stimulus compatible with cell viability.[24] Under these conditions, photostimulation emerges as a minimally invasive yet highly effective method for driving muscle contraction.

As a final note, using the average active tension generated by a single myotube ($F_{sm} = 0.88$ µN),[54] we estimate that producing 460 µN of force requires roughly 523 contractile myotubes. Given our electrospun membrane dimensions, the total volume is about 3.5 mm^3; accounting for porosity, the available volume for cell growth and differentiation ($\varphi \approx 0.641$) reduces roughly 2 mm^3. With an average myotube measuring 20 µm in diameter[57] and 300 µm in length,[58] each occupies approximately 1×10^{-4} mm^3, so all 523 active myotubes together fill about 0.05 mm^3, which is the 2.5 percent of the scaffold's available space. This occupancy highlights substantial room for increasing cell density and alignment, and thus contractile output, through optimized seeding strategies, scaffold design, or extended culture protocols.

Conclusions

In this work, we demonstrate that electrospun PVA nanofiber membranes provide a quasi-3D microenvironment that supports C2C12 alignment and enables macroscopic force generation. The aligned fiber architecture provides contact guidance through its anisotropic structure, promoting parallel cellular organization and increasing the formation of elongated, multinucleated structures, as quantified by orientation analysis and fusion index measurements. While definitive confirmation of myogenic differentiation would require comprehensive molecular characterization (e.g., immunostaining for structural proteins and gene expression analysis), the present study was primarily focused on materials design and functional scaffold performance. Within this framework, the observation of organized, multinucleated cellular assemblies capable of spontaneous and light-induced contractions supports the development of a biohybrid photoactuation platform.

Implementation of the membranes as free-standing constructs enables volumetric cell organization, as demonstrated by confocal z-stack imaging showing nuclei distributed throughout the membrane thickness, consistent with a three-dimensional cellular arrangement within the porous fibrous network. In parallel, in situ mechanical testing established that hydrated membranes exhibit an elastic modulus of approximately 8 MPa, providing mechanically robust support for handling and actuation under physiological conditions.

Functionally, optical stimulation of Ziapin2-infiltrated membranes under visible light produces reproducible construct

Table 1 Summary of the ES PVA aligned self-standing membrane average parameters used for the force calculation. The displacement is obtained upon optical stimulation at 470 nm (42 mW mm^{-2}) and with a frequency of 1 Hz. Here, we report the best performances for both, while other values are reported in Fig. S13 in the SI

Sample	Thickness (µm)	Length (mm)	Width (mm)	ΔL_0 (µm)	E (MPa)	A_0 (mm^2)	A_{ef} (mm^2)	σ_0 (kPa)
PVA aligned	35 ± 3	10	10	3.5 ± 0.4	8.26 ± 3	0.35	0.14	2.9 ± 0.3

This journal is © The Royal Society of Chemistry 2026

J. Mater. Chem. B, 2026, **14**, 2832–2842 | **2839**

contractions (displacements ~ 4 μm), corresponding to estimated forces up to ~ 460 μN and stresses up to ~ 3.3 kPa based on measured displacement and scaffold mechanical parameters. Although only a fraction of the available scaffold volume appears occupied by contractile cellular assemblies, suggesting opportunities for further optimization of cell density and maturation, these results establish free-standing electrospun nanofiber membranes as a versatile platform for light-addressable muscle-like constructs with potential applications in soft bioactuation, drug screening, *in vitro* modelling, and regenerative medicine.

Author contributions

Conceptualization: G. S. and G. L.; methodology: G. S., I. V., F. M. and V. V.; synthesis: P. M., M. R. and C. B.; validation: G. S.; formal analysis: G. S., G. M. P. and G. L.; investigation: G. S., A. B., L. V. and L. A.; data curation: G. S., G. M. P. and G. L.; writing – original draft: G. S.; writing – review & editing: G. S., F. M., V. V., A. B., L. V., G. M. P and G. L.; visualization: G. S.; supervision: G. M. P., C. B. and G. L.; project administration: G. S. and G. L.; funding acquisition: G. L.

Conflicts of interest

The authors declare that they have no competing interests.

Data availability

All resources used in this work are included in the published article and its supplemental information (SI) files. The data contained in this paper can be found here: https://doi.org/10.5281/zenodo.15727910. Supplementary information is available. See DOI: https://doi.org/10.1039/d5tb02640g.

Acknowledgements

References

1 S. Pacilio, *et al.*, Electrospun Poly(L-lactide-*co*-ε-caprolactone) Scaffold Potentiates C2C12 Myoblast Bioactivity and Acts as a Stimulus for Cell Commitment in Skeletal Muscle Myogenesis, *Bioengineering*, 2023, **10**, 239.

2 N. G. Kozan, M. Joshi, S. T. Sicherer and J. M. Grasman, Porous biomaterial scaffolds for skeletal muscle tissue engineering, *Front. Bioeng. Biotechnol.*, 2023, **11**, 1245897.

3 C.-Y. Lo, *et al.*, Highly stretchable self-sensing actuator based on conductive photothermally-responsive hydrogel, *Mater. Today*, 2021, **50**, 35–43.

4 C. Florindi, G. Simoncini, G. Lanzani and F. Lodola, Shining light in a heartbeat: Controlling cardiac bioelectricity with membrane-targeted photoswitches, *Appl. Phys. Lett.*, 2025, **126**, 230501.

5 C. Chen, W. Hou and X. He, NeuroMuscles: Pioneering materials open a new path to artificial skeletal muscles, *Matter*, 2025, **8**, 102031.

6 M. Li, A. Pal, A. Aghakhani, A. Pena-Francesch and M. Sitti, Soft actuators for real-world applications, *Nat. Rev. Mater.*, 2022, **7**, 235–249.

7 F. Ershad, *et al.*, Bioprinted optoelectronically active cardiac tissues, *Sci. Adv.*, 2025, **11**, eadt7210.

8 A. M. Almonacid Suarez, Q. Zhou, P. van Rijn and M. C. Harmsen, Directional topography gradients drive optimum alignment and differentiation of human myoblasts, *J. Tissue Eng. Regener. Med.*, 2019, **13**, 2234–2245.

9 S. H. Ku, S. H. Lee and C. B. Park, Synergic effects of nanofiber alignment and electroactivity on myoblast differentiation, *Biomaterials*, 2012, **33**, 6098–6104.

10 A. Bettadapur, *et al.*, Prolonged Culture of Aligned Skeletal Myotubes on Micromolded Gelatin Hydrogels, *Sci. Rep.*, 2016, **6**, 28855.

11 W. Mao, S. Lee, S.-R. Kim, K.-N. Kim and H. S. Yoo, Electrospun nanohybrid hydrogels for enhanced differentiation of myoblasts, *J. Ind. Eng. Chem.*, 2019, **80**, 838–845.

12 S. Pacilio, *et al.*, Electrospun Poly(L-lactide-*co*-ε-caprolactone) Scaffold Potentiates C2C12 Myoblast Bioactivity and Acts as a Stimulus for Cell Commitment in Skeletal Muscle Myogenesis, *Bioengineering*, 2023, **10**, 239.

13 Z. Ma, M. Kotaki, R. Inai and S. Ramakrishna, Potential of Nanofiber Matrix as Tissue-Engineering Scaffolds, *Tissue Eng.*, 2005, **11**, 101–109.

14 R. Balint, N. J. Cassidy and S. H. Cartmell, Electrical Stimulation: A Novel Tool for Tissue Engineering, *Tissue Eng., Part B*, 2013, **19**, 48–57.

15 V. Vurro, I. Venturino and G. Lanzani, A perspective on the use of light as a driving element for bio-hybrid actuation, *Appl. Phys. Lett.*, 2022, **120**, 080502.

16 L. Aloisio, *et al.*, Insight on the Intracellular Supramolecular Assembly of DTTO: A Peculiar Example of Cell-Driven Polymorphism, *Adv. Mater.*, 2023, **35**, 2302756.

17 T. Asano, T. Ishizua and H. Yawo, Optically controlled contraction of photosensitive skeletal muscle cells, *Biotechnol. Bioeng.*, 2012, **109**, 199–204.

18 T. Bruegmann, *et al.*, Optogenetic control of contractile function in skeletal muscle, *Nat. Commun.*, 2015, **6**, 7153.

19 R. Raman, *et al.*, Optogenetic skeletal muscle-powered adaptive biological machines, *Proc. Natl. Acad. Sci. U. S. A.*, 2016, **113**, 3497–3502.

20 A Polymer Blend Substrate for Skeletal Muscle Cells Alignment and Photostimulation - Vurro - 2021 - Advanced Photonics Research - Wiley Online Library. https://advanced.onlinelibrary.wiley.com/doi/full/10.1002/adpr.202000103.

2840 | *J. Mater. Chem. B*, 2026, **14**, 2832–2842

This journal is © The Royal Society of Chemistry 2026

21 F. Lodola, V. Vurro, S. Crasto, E. Di Pasquale and G. Lanzani, Optical Pacing of Human-Induced Pluripotent Stem Cell-Derived Cardiomyocytes Mediated by a Conjugated Polymer Interface, *Adv. Healthcare Mater.*, 2019, **8**, e1900198.

22 A. Savchenko, *et al.*, Graphene biointerfaces for optical stimulation of cells, *Sci. Adv.*, 2018, **4**, eaat0351.

23 E. Ganji, C. S. Chan, C. W. Ward and M. L. Killian, Optogenetic activation of muscle contraction in vivo, *Connect. Tissue Res.*, 2021, **62**, 15–23.

24 I. Venturino, *et al.*, Skeletal muscle cells opto-stimulation by intramembrane molecular transducers, *Commun. Biol.*, 2023, **6**, 1148.

25 R. Rizzi, *et al.*, Tissue engineering for skeletal muscle regeneration, *Muscles Ligaments Tendons J.*, 2012, **2**, 230–234.

26 J. Wang, *et al.*, Engineered skeletal muscles for disease modeling and drug discovery, *Biomaterials*, 2019, **221**, 119416.

27 J. Wang, Y. Wang, Y. Kim, T. Yu and R. Bashir, Multi-actuator light-controlled biological robots, *APL Bioeng.*, 2022, **6**, 036103.

28 M. A. Teixeira, M. T. P. Amorim and H. P. Felgueiras, Poly(Vinyl Alcohol)-Based Nanofibrous Electrospun Scaffolds for Tissue Engineering Applications, *Polymers*, 2020, **12**, 7.

29 M. Janmohammadi and M. S. Nourbakhsh, Electrospun polycaprolactone scaffolds for tissue engineering: a review, *Int. J. Polym. Mater. Polym. Biomater.*, 2019, **68**, 527–539.

30 K. Molnar, *et al.*, Biocompatibility study of poly(vinyl alcohol)-based electrospun scaffold for hernia repair, *eXPRESS Polym. Lett.*, 2018, **12**, 676–687.

31 Y. Z. Zhang, J. Venugopal, Z.-M. Huang, C. T. Lim and S. Ramakrishna, Characterization of the Surface Biocompatibility of the Electrospun PCL-Collagen Nanofibers Using Fibroblasts, *Biomacromolecules*, 2005, **6**, 2583–2589.

32 P. Veliça and C. M. Bunce, A quick, simple and unbiased method to quantify C2C12 myogenic differentiation, *Muscle Nerve*, 2011, **44**, 366–370.

33 V. Vurro, *et al.*, Molecular Design of Amphiphilic Plasma Membrane-Targeted Azobenzenes for Nongenetic Optical Stimulation, *Front. Mater.*, 2021, **7**, 631567.

34 G. M. Paternò, *et al.*, Membrane Environment Enables Ultrafast Isomerization of Amphiphilic Azobenzene, *Adv. Sci.*, 2020, **7**, 1903241.

35 V. Vurro, A. Magni, L. Aloisio and G. Lanzani, Photostimulation mechanism of an amphiphilic azobenzene, *Il Nuovo Cimento C*, 2023, **46**, 1–4.

36 C. Vesga-Castro, J. Aldazabal, A. Vallejo-Illarramendi and J. Paredes, Contractile force assessment methods for in vitro skeletal muscle tissues, *eLife*, 2022, **11**, e77204.

37 C. F. Guimarães, L. Gasperini, A. P. Marques and R. L. Reis, The stiffness of living tissues and its implications for tissue engineering, *Nat. Rev. Mater.*, 2020, **5**, 351–370.

38 D. Kah, *et al.*, Contractility of cardiac and skeletal muscle tissue increases with environmental stiffness, 2024.02.23.581737 Preprint at https://doi.org/10.1101/2024.02.23.581737 (2024).

39 P. Bajaj, *et al.*, Patterning the differentiation of C2C12 skeletal myoblasts, *Integr. Biol.*, 2011, **3**, 897–909.

40 M. Zocchi, D. Béchet, A. Mazur, J. A. Maier and S. Castiglioni, Magnesium Influences Membrane Fusion during Myogenesis by Modulating Oxidative Stress in C2C12 Myoblasts, *Nutrients*, 2021, **13**, 1049.

41 M. Chakraborty, A. Sivan, A. Biswas and B. Sinha, Early tension regulation coupled to surface myomerger is necessary for the primary fusion of C2C12 myoblasts, *Front. Physiol.*, 2022, **13**, 976715.

42 N. R. W. Martin, *et al.*, Factors affecting the structure and maturation of human tissue engineered skeletal muscle, *Biomaterials*, 2013, **34**, 5759–5765.

43 F. J. Calero-Castro, *et al.*, Mechanical Stimulation and Aligned Poly(ε-caprolactone)–Gelatin Electrospun Scaffolds Promote Skeletal Muscle Regeneration, *ACS Appl. Bio Mater.*, 2024, **7**, 6430–6440.

44 M. Moschetta, *et al.*, Modulation of Mechanosensitive Potassium Channels by a Membrane-targeted Nongenetic Photoswitch, *J. Phys. Chem. B*, 2023, **127**, 8869–8878.

45 T. A. McBride, B. W. Stockert, F. A. Gorin and R. C. Carlsen, Stretch-activated ion channels contribute to membrane depolarization after eccentric contractions, *J. Appl. Physiol.*, 2000, **88**, 91–101.

46 T. C. de Souza-Guerreiro, *et al.*, Membrane Targeted Azobenzene Drives Optical Modulation of Bacterial Membrane Potential, *Adv. Sci.*, 2023, **10**, 2205007.

47 M. L. DiFrancesco, *et al.*, Neuronal firing modulation by a membrane-targeted photoswitch, *Nat. Nanotechnol.*, 2020, **15**, 296–306.

48 V. Vurro, *et al.*, Light-triggered cardiac microphysiological model, *APL Bioeng.*, 2023, **7**, 026108.

49 V. Vurro, *et al.*, Optical modulation of excitation-contraction coupling in human-induced pluripotent stem cell-derived cardiomyocytes, *iScience*, 2023, **26**, 106121.

50 S. A. Riboldi, M. Sampaolesi, P. Neuenschwander, G. Cossu and S. Mantero, Electrospun degradable polyesterurethane membranes: potential scaffolds for skeletal muscle tissue engineering, *Biomaterials*, 2005, **26**, 4606–4615.

51 W. Chen, X. Tao, P. Xue and X. Cheng, Enhanced mechanical properties and morphological characterizations of poly(vinyl alcohol)–carbon nanotube composite films, *Appl. Surf. Sci.*, 2005, **252**, 1404–1409.

52 D. S. Jones, J. Djokic, C. P. McCoy and S. P. Gorman, Poly(ε-caprolactone) and poly(ε-caprolactone)-polyvinylpyrrolidone-iodine blends as ureteral biomaterials: characterisation of mechanical and surface properties, degradation and resistance to encrustation in vitro, *Biomaterials*, 2002, **23**, 4449–4458.

53 T. Diwan, Z. N. Abudi, M. H. Al-Furaiji and A. Nijmeijer, A Competitive Study Using Electrospinning and Phase Inversion to Prepare Polymeric Membranes for Oil Removal, *Membranes*, 2023, **13**, 474.

54 B. Yan, Y. Zhang, Z. Li, P. Zhou and Y. Mao, Electrospun nanofibrous membrane for biomedical application, *SN Appl. Sci.*, 2022, **4**, 172.

This journal is © The Royal Society of Chemistry 2026

J. Mater. Chem. B, 2026, **14**, 2832–2842 | **2841**

55 F. E. Mustafa and B.-K. Lee, Improved Mechanical Stability and Regulated Gentamicin-Release of Polyvinyl Alcohol/Chitosan Nanofiber Membranes *via* Heat Treatment, *J. Biomed. Mater. Res. A*, 2025, **113**, e37905.

56 H. Fujita, K. Shimizu and E. Nagamori, Novel method for measuring active tension generation by C2C12 myotube using UV-crosslinked collagen film, *Biotechnol. Bioeng.*, 2010, **106**, 482–489.

57 C. M. Girgis, R. J. Clifton-Bligh, N. Mokbel, K. Cheng and J. E. Gunton, Vitamin D Signaling Regulates Proliferation, Differentiation, and Myotube Size in C2C12 Skeletal Muscle Cells, *Endocrinology*, 2014, **155**, 347–357.

58 S. Ostrovidov, *et al.*, Three-dimensional co-culture of C2C12/PC12 cells improves skeletal muscle tissue formation and function, *J. Tissue Eng. Regener. Med.*, 2017, **11**, 582–595.

2842 | *J. Mater. Chem. B*, 2026, **14**, 2832–2842

This journal is © The Royal Society of Chemistry 2026